Chapter

Modeling Lost-Circulation into Fractured Formation in Rock Drilling Operations

Rami Albattat and Hussein Hoteit

Abstract

Loss of circulation while drilling is a challenging problem that may interrupt drilling operations, reduce efficiency, and increases cost. When a drilled borehole intercepts conductive faults or fractures, lost circulation manifests as a partial or total escape of drilling, workover, or cementing fluids into the surrounding rock formations. Studying drilling fluid loss into a fractured system has been investigated using laboratory experiments, analytical modeling, and numerical simulations. Analytical modeling of fluid flow is a tool that can be quickly deployed to assess lost circulation and perform diagnostics, including leakage rate decline and fracture conductivity. In this chapter, various analytical methods developed to model the flow of non-Newtonian drilling fluid in a fractured medium are discussed. The solution methods are applicable for yield-power-law, including shear-thinning, shear-thickening, and Bingham plastic fluids. Numerical solutions of the Cauchy equation are used to verify the analytical solutions. Type-curves are also described using dimensionless groups. The solution methods are used to estimate the range of fracture conductivity and time-dependent fluid loss rate, and the ultimate total volume of lost fluid. The applicability of the proposed models is demonstrated for several field cases encountering lost circulations.

Keywords: lost-circulation, mud loss, leakage, fractures, Herschel-Bulkley, yield-power law, Cauchy momentum equation, type-curves, non-Newtonian fluids

1. Introduction

Drilling technology has been widely deployed in many industries, such as oil and gas, geothermal, environmental remediation, mining, carbon dioxide sequestration, gas storage, water well, infrastructure development, among others [1]. In many situations, drilling entails various technical challenges and difficulties, often causing economic, safety, and environmental disturbances. Due to the complex nature of subsurface geological formations, technical problems often emerge unexpectedly. One of the most pressing problems is lost circulation into fractured formation. Preserving the drilling fluid within the borehole is crucial for removing cuttings, lubrication, hydraulic rotations, pressure control, among others. Fluid total or partial loss into the wellbore surrounding formation may result in wellbore instability.

Drilling fluid-loss is a costly problem. This phenomenon may obstruct operations, increase the nonproductive time (NPT), contaminate water tables, and cause formation damage and safety hazard [2–9]. Drilling fluid typically accounts for

25–40% of the total drilling costs [8]. Furthermore, lost circulation may cause other issues, such as wellbore instability, sloughing shale, and washout [10]. Such problems cost the industry about one billion US dollars per annum worldwide [11, 12]. For instance, a study including 1500 gas wells in the Gulf of Mexico showed that lost-circulation accounts for 13% of the total drilling problems [5], as appears in **Figure 1**. Another study for 103 wells in the Duvernay area in Canada reported a loss of $2.6 million and 27.5 days of NPT because of lost circulation (**Figure 2**). In the Middle East, a group of 144 wells in Rumaila field, Iraq, encountered major lost-circulation problems [14], causing 48% of all drilling issues and loss of 295 days NPT, as illustrated in **Figure 3**. This high occurrence of lost-circulation was attributed to the presence of conductive natural fractures in the carbonate formations. For instance, more than 35% of drilled wells in a fractured carbonate formation in Iran experienced lost circulation [15]. Similarly, in Saudi Arabia, one-third of the

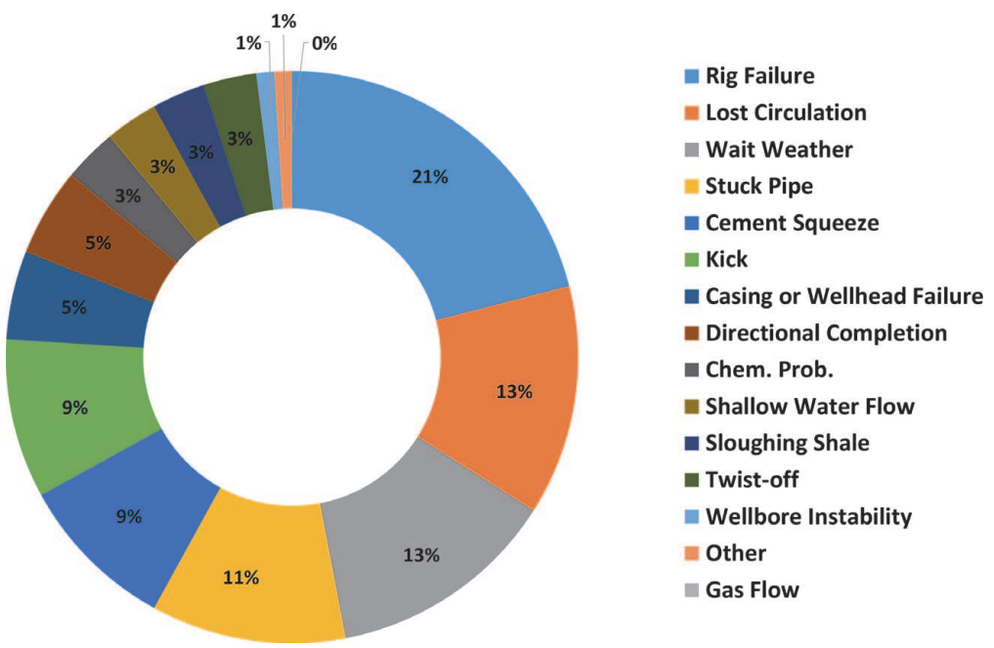

Figure 1.
Contribution of various drilling problems reported for 1500 wells in the Gulf of Mexico [5], where lost circulation accounts for 13% of the total.

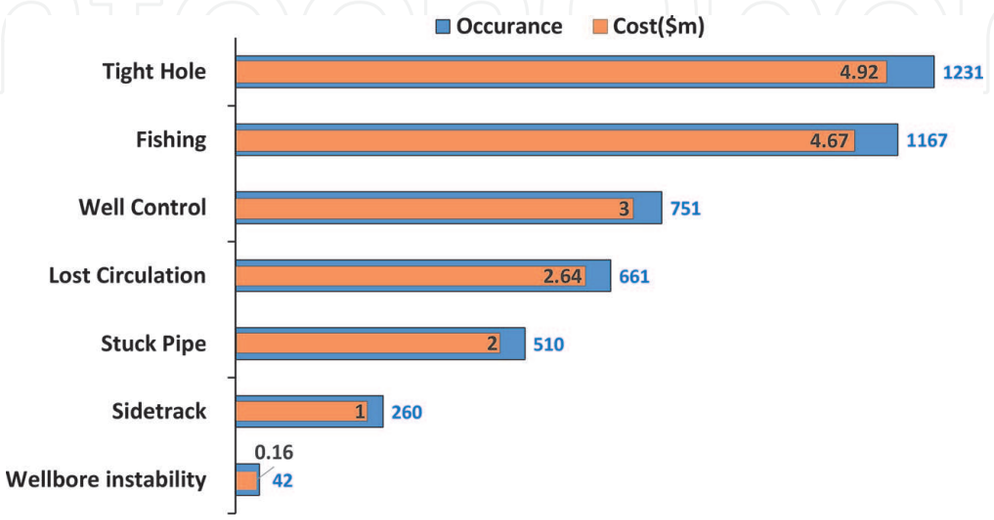

Figure 2.
Cost overhead from various drilling problems for 103 wells in the Duvernay area in Canada [13], where lost circulation account for $2.6 m.

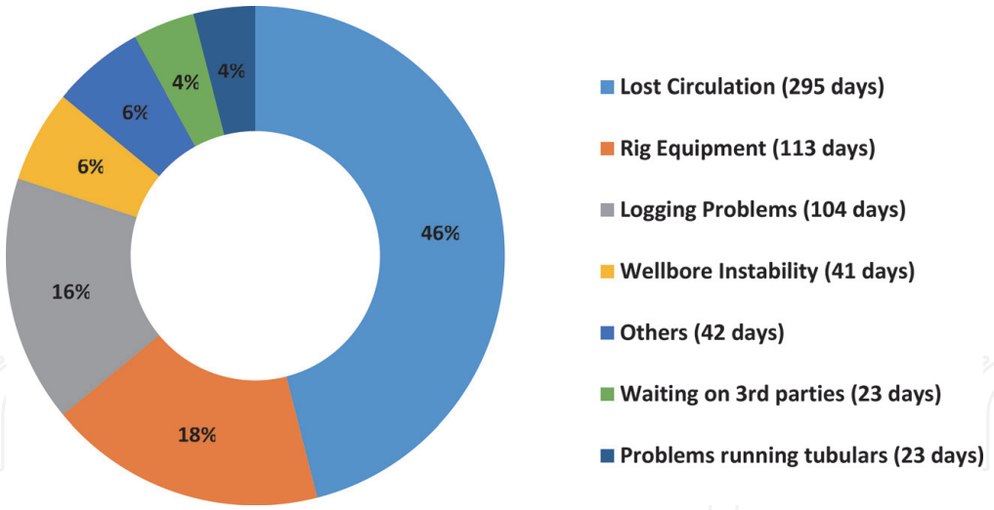

Figure 3.
Contribution of various drilling problems to NPT in the Rumaila field in Iraq, total lost circulation is the top drilling issue encountered in that field, data source from [14].

drilled well underwent lost circulation [16]. Lost circulation has also been reported in other places [17, 18].

Lost circulation can be classified based on the severity of the flow loss rate [19], as shown in **Table 1**. These categories provide general guidance to set the mitigation plan depending on the severity of the fluid loss. Seepage loss can sometimes be tolerable to continue drilling without interruption. However, major loss demands a careful response to regain a full circulation fluid.

Fluid loss is often encountered in fractured formations, which can be subdivided into four types: induced-drilling fracture, caves or vugs, natural fracture, and high permeable formation [20]. An illustration of the four types is shown in **Figure 4**. Each formation type exhibits different fluid loss behavior and, therefore, may require a specific mitigation plan.

Naturally fractured formation, which is the focus of this chapter, is often prone to severe loss during either drilling, cementing, or completion/workover job [21]. Consequently, multiple problems may emanate because of the loss severity, such as kicks, wellbore instability, environmental contamination, and formation damage. To mitigate this problem, one procedure is to add lost circulation material (LCM) to the circulation fluid [22–25]. The LCM fluid properties such as viscosity and density are selected according to the formation type and the subsurface conditions, such as the depth, pressure, and fracture conductivity, among other factors [26]. Fluid loss rate into natural fractures mostly commences with a sudden spurt followed by a gradual declining loss [27]. The ultimately lost volume is dependent on several factors, such as fluid mobility, fracture conductivity, pore-volume, and fracture extension [28].

Because of the nature of this problem that requires immediate intervention, there is a need in the industry to establish an accurate and efficient modeling tool

Lost Type	Flow Rate Amount
Seepage loss	Less than 1.5 m^3/hr
Partial loss	1.5 to 15 m^3/hr
Severe loss	15 to 75 m^3/hr
Total loss	No return to surface

Table 1.
Classification of lost-circulation severity [19].

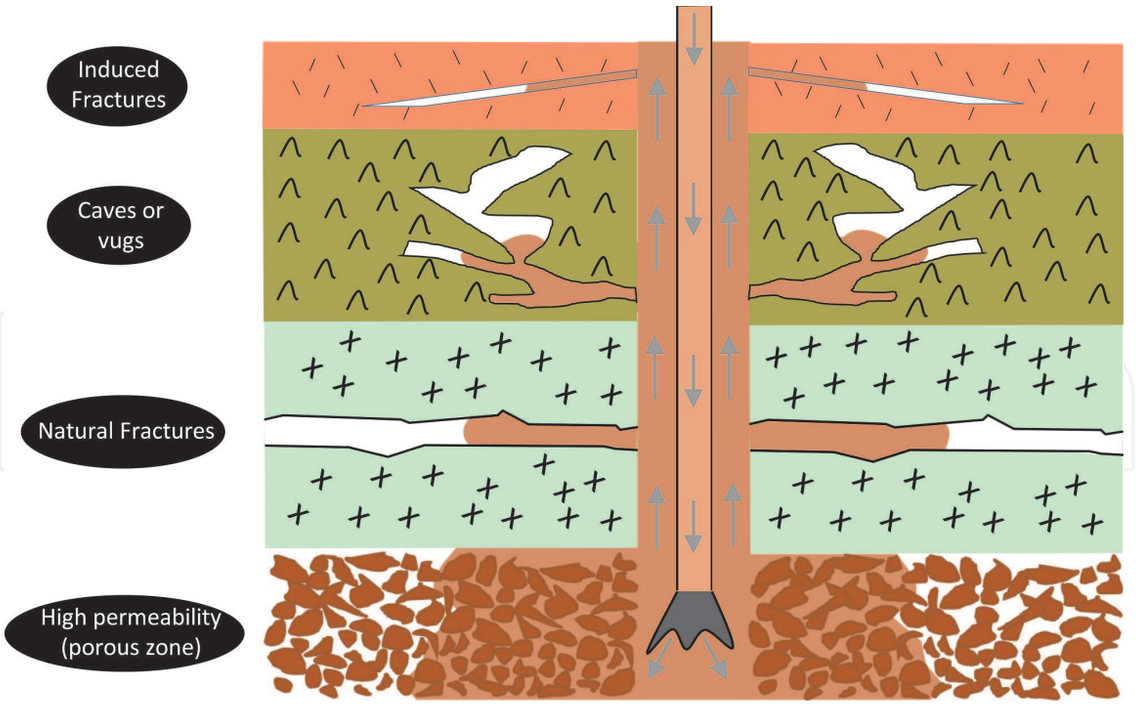

Figure 4.
Four types of rock formations causing loss-circulation. The arrows indicate the direction of circulating fluid starting from the surface within the drill pipe going to the open-hole and to the annulus of the wellbore back to the surface.

that is feasible at real-time drilling operations to perform diagnostics and predictions.

During the last two decades, many analytical solutions have been introduced in the literature to model mud loss into fractured formation. Early modeling attempts for simplified fractured cases were based on Darcy's Law at steady-state conditions [29, 30]. Afterward, a semi-analytical solution was introduced for the Newtonian fluid model into a horizontal fracture by combining the diffusivity equation and mass conservation in a one-dimensional (1D) radial system [31]. Since this derived ordinary differential equation (ODE) was solved numerically, an analytical solution of the diffusivity equation for a fluid with a constant viscosity at steady-state conditions was introduced [32]. Another approach based on type-curves, which were generated by numerical solutions to describe mud loss volume as a function of time into a horizontal fracture, was established [33]. The type-curves are applicable for non-Newtonian fluid and follow a model that exhibits Bingham plastic rheological behavior. The numerically generated type-curves are based on dimensionless parameters that depend on the effective fracture hydraulic aperture, fluid properties, and differential pressure. However, these models inherit the limitations of numerical methods in introducing numerical artifacts such as numerical dispersion and grid dependency. Later, an analytical solution was proposed [34, 35]. Estimation of hydraulic fracture aperture by simplifying insignificant terms in the final equation form was analyzed [36]. Following the same workflow, a solution was developed based on Yield-Power-Law fluid by reducing a Taylor expansion of the governing nonlinear flow equation into its linear terms [37].

This chapter is intended to give an overview of laboratory and modeling tools applicable for lost circulation in fractured media. Two main subjects are discussed. First, the governing equations to model non-Newtonian fluid in a fractured system are reviewed. We then introduce the solution method to develop a semi-analytical solution to model drilling fluid loss. The fluid exhibits a Herschel-Bulkley behavior, where the Cauchy equation of motion is used to describe the fluid flow. Due to the

nonlinearity of the problem, the system of equations is reformulated and transformed into ODE's, which is then computed numerically with an efficient ODE solver [38]. Based on the semi-analytical solution, type-curves are generated, capturing dimensionless fluid loss volume as a function of time. High-resolution finite element methods are used to verify the analytical approach. The applicability of the method is then demonstrated for field cases exhibiting loss of circulation, where formation and fluid uncertainties are addressed with Monte Carlo simulations. In the second subject, an experimental study designed to mimic fluid leakage in a horizontal fracture is discussed. These experiments are used to study the steady-state flow conditions of non-Newtonian fluids into the fracture and demonstrate the flow stoppage process. Simulations are used to replicate the physics, including the effect of fracture deformation. Type-curves are also derived from Cauchy equation of motion to capture the effect of fracture ballooning.

2. Mud invasion into a fractured system

Various studies have been conducted in the literature to investigate the flow behavior of drilling fluids in fractured systems [39–41], where a horizontal, radial fracture is considered, as shown in **Figure 5**. The choice of the fracture geometry is motivated by its convenience to be replicated with experimental apparatus and analytical modeling. Even though the fracture geometry may seem simplistic, it can provide useful insights at lab and field scales [43, 44].

Consider two parallel radial plates to mimic a horizontal fracture, intercepting a wellbore, as illustrated in **Figure 5**. Note that horizontal fractures could occur at shallow depths and over-pressurized formations [45, 46].

The general governing equation describing the dynamics of non-Newtonian fluid flow in an open fracture is given by the Cauchy momentum Equation [47, 48], such that,

$$\rho \frac{\partial \mathbf{v}}{\partial t} + \rho(\mathbf{v} \cdot \nabla)\mathbf{v} = \nabla \cdot (-p\mathbf{I} + \boldsymbol{\tau}) + \rho \mathbf{g}, \tag{1}$$

Where p denotes the fluid pressure, t is time, $\boldsymbol{\tau}$ is the shear stress, $\mathbf{g}$ is the gravity term, ρ is the density, $\mathbf{I}$ is identity matrix, and $\mathbf{v}$ is the flow velocity. Divergence delta operator is $\nabla\cdot$.

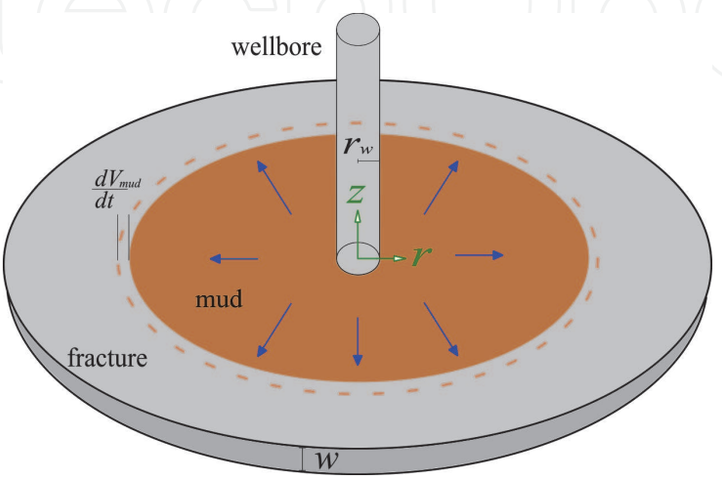

Figure 5.
Physical domain illustrating a horizontal fracture intercepted by a wellbore. The shaded brown area reflects the invaded mud zone, r_w is the wellbore radius, w is the fracture aperture, V_{mud} is the mud loss volume, and t is the time [42].

Assuming steady-state conditions and neglecting the gravity and inertial effects, Eq. (1) simplifies to,

$$0 = \nabla \cdot (-p\mathbf{I} + \boldsymbol{\tau}), \tag{2}$$

The above equation reduces into two fundamental forces; pressure forces and shear stress force. In a 1D radial system with polar coordinates, Eq. (2) simplifies to (see [49]),

$$\tau(z, r) = z\frac{\partial p}{\partial r}, \tag{3}$$

Where $\tau(z, r)$ is the radial shear stress component perpendicular to the z-directionand r is radial distance which is the variable argument.

On the other hand, the Herschel-Bulkley model is expressed by [50],

$$\tau(z, r) = \tau_0 + m\left(\frac{dv_r}{dz}\right)^n. \tag{4}$$

The fluid yield stress, which determines the fluidity state, is denoted by τ_0, and the consistency multiplier and behavioral flow index are $m$and n, respectively. The flow index is a positive number, reflecting the fluid rheological behavior where shear-thinning ($n < 1$) and shear-thickening ($n > 1$) can occur. Typical values of this dimensionless parameter for drilling fluids range from 0.3 to 1.0 [51]. Shear rate, which is the derivative of the radial velocity v_r in the z-direction, is nonlinear due to the flow index.

The mechanisms corresponding to the solution method of the mud invasion phenomenon in a fractured system are shown on a cross-section in **Figure 6**. The radial velocity decreases as the fluid propagates away from the wellbore within the fracture, and therefore shear stress lessens. Therefore, shear-thinning is expected to be maximum near the wellbore and reduces gradually with radial distance, which induces shear-thickening from yield stress. Furthermore, flow velocity and shear stress variations in the z-direction create layers of fluid rheological properties and fluid self-friction that becomes maximum at the walls of the fracture. Fluid self-friction is minimum at the centerline of the fracture, as shown in **Figure 6**, resulting in a region at the fracture center with zero shear rate, that is, $dv_r/dz = 0$. In this zone, the yield shear stress corresponds to τ_0(see Eq. (4)). This fluid flow region in the fracture is subdivided into plug-flow and free-flow regions. The plug-region extends toward the walls of the fracture as the shear-stress reduces, and the fluid flows further from the wellbore. The plug region can eventually reach the fracture wall leading to a complete stoppage of the fluid leakage (see **Figure 7a**). In other words,

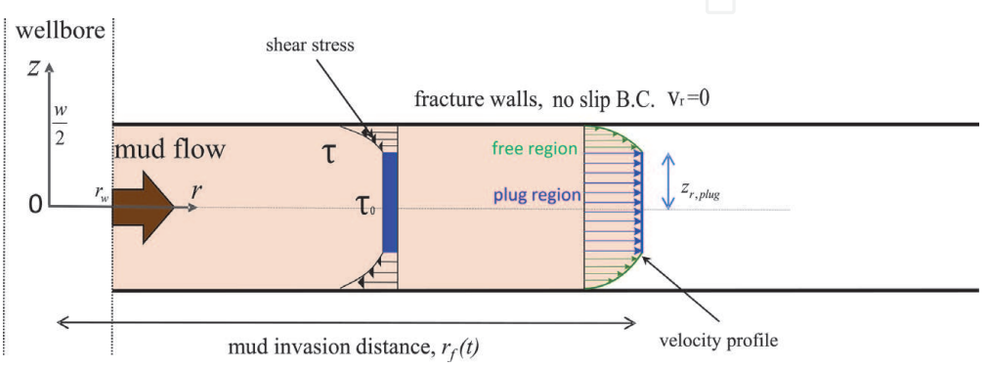

Figure 6.
Illustration of an infinite-acting fracture of aperture w, intercepting a wellbore with radius r_w. No-flow and no-slip boundary conditions are imposed at the fracture wall. Mud-front distance $r_f(t)$ is a time-dependent parameter.

mud leakage stalls in the fracture when the pressure gradient between the fracture inlet and the mud front becomes smaller than the yield stress τ_0 (see **Figure 7b**).

The following boundary conditions are considered for the two flow regions,

$$v_r(z) = \begin{cases} v_{r,plug}(z), & for \quad z \le z_{plug} \\ v_{r,free}(z), & for \quad z_{plug} < z < \dfrac{w}{2} \\ 0, & for \quad z = \dfrac{w}{2} \end{cases} \tag{5}$$

In the above equation, z_{plug} represents the extension of the plug region in the z-direction. $v_{r,plug}$, and $v_{r,free}$ are, respectively, the flow velocities within the plug- and free-region. The no-slip boundary condition is described by the last equation in (5).

Eq. (4) and Eq. (3) are combined to express the solution of the velocity, such that,

$$v_r(z) = \frac{n\left(-\frac{\partial p}{\partial r}\frac{w}{2} + \tau_0\right)\left(\frac{\frac{\partial p_w}{\partial r}2 - \tau_0}{m}\right)^{1/n} + n\left(-\frac{\partial p}{\partial r}z + \tau_0\right)\left(\frac{\frac{\partial p}{\partial r}z - \tau_0}{m}\right)^{\frac{1}{n}}}{\frac{\partial p}{\partial r}(n+1)} \tag{6}$$

The plug-region is modeled by imposing the condition, $dv_r/dz = 0$. Therefore, Eq. (6) can be expressed for each region individually, as follows,

$$\begin{aligned} v_{r,free}(z) &= \frac{n}{n+1}\left(z_{plug} - \frac{w}{2}\right)\left(\frac{\frac{\partial p}{\partial r}\left(\frac{w}{2} - z_{plug}\right)}{m}\right)^{1/n} + \frac{n}{n+1}\left(z - z_{plug}\right)\left(\frac{\frac{\partial p}{\partial r}\left(z - z_{plug}\right)}{m}\right)^{\frac{1}{n}} \\ v_{r,plug}(z) &= \frac{n}{n+1}\left(\frac{\tau_0}{\frac{\partial p}{\partial r}} - \frac{w}{2}\right)\left(\frac{\left(\frac{w}{2}\frac{\partial p}{\partial r} - \tau_0\right)}{m}\right)^{1/n} \end{aligned} \tag{7}$$

From the definition of the total volumetric flow rate Q_{total}, one obtains,

$$Q_{total} = Q_{plug} + Q_{free} \tag{8}$$

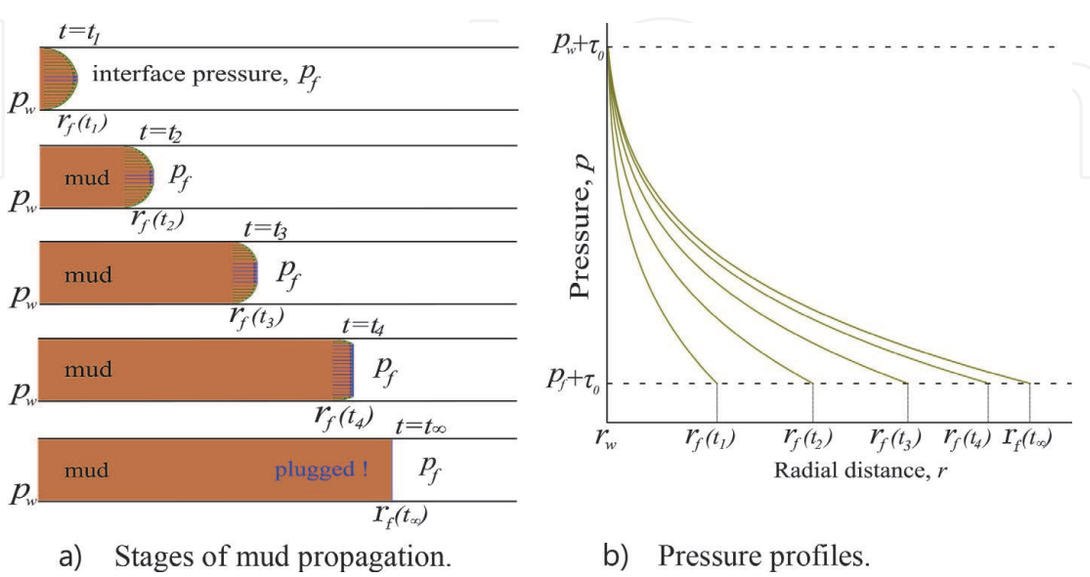

Figure 7.
Illustration of yield-power-law fluid flow in a radial fracture showing the evolution of the propagation of the plug region as the mud travels away from the wellbore, resulting in total plugging (a). Plot (b) shows typical pressure profiles versus radial distance at various times and invasion distances.

Applying surface integral,

$$Q_{total} = 4\pi r \int_{0}^{z_{plug}} v_{r,plug} dz + 4\pi r \int_{z_{plug}}^{w/2} v_{r,free} dz \tag{9}$$

Substituting Eq. (7) into Eq. (9) and arranging to obtain,

$$Q_{total}^{n} = \frac{(4\pi r)^{n}}{m}\left(\frac{w}{2}\right)^{2n+1}\left(\frac{n}{2n+1}\right)^{n}\left(\frac{dp}{dr}\right)\left(1-\frac{\tau_0}{\frac{w}{2}\frac{dp}{dr}}\right)\left(1-\left(\frac{1}{n+1}\right)\frac{\tau_0}{\frac{w}{2}\frac{dp}{dr}}-\left(\frac{n}{n+1}\right)\left(\frac{\tau_0}{\frac{w}{2}\frac{dp}{dr}}\right)^{2}\right)^{n} \tag{10}$$

The above equation is rearranged with the following quadratic equation to express the pressure term explicitly, that is,

$$\left(\frac{dp}{dr}\right)^{2} - \left(\frac{Q_{total}^{n}}{r^{n}A} + B\right)\frac{dp}{dr} + D = 0 \tag{11}$$

Where,

$$A = \frac{(4\pi)^{n}}{m}\left(\frac{w}{2}\right)^{2n+1}\left(\frac{n}{2n+1}\right)^{n}; B = \left(\frac{2n+1}{n+1}\right)\frac{\tau_0}{w/2}; D = \left(\frac{n-n^{2}}{n+1}\right)\left(\frac{\tau_0}{w/2}\right)^{2}$$

Solving the differential pressure and integrating along the radial domain by implementing a moving boundary condition, a final ODE system is reached, as follows,

$$\begin{cases} p_f - p_w = \dfrac{B\left(r_f(t) - r_w\right)}{2} + \dfrac{Q_{total}^{n}\left(r_f(t)^{1-n} - r_w^{1-n}\right)}{2(1-n)A} + \dfrac{1}{2}\displaystyle\int_{r_w}^{r_f(t)}\left(\sqrt{\left(B + \frac{Q_{total}^{n}}{r^{n}A}\right)^{2} - 4D}\right)dr \\ Q_{total} = 2\pi w r_f(t)\dfrac{dr_f(t)}{dt} \end{cases} \tag{12}$$

Eq. (12) is nonlinear for a general value of n, and it cannot be solved analytically. However, a general semi-analytical solution can be derived [42]. This solution is a generalization to other particular solutions in the literature. For instance, when $n = 1$, reflecting a Bingham plastic fluid, a closed-form solution can be obtained, as demonstrated by Lietard *et al.* [33]. **Figure 8** shows that the proposed general semi-analytical solution is in perfect agreement with the analytical solution by Lietard *et al.* [33]. For general cases of n, numerical simulations could be used to verify the semi-analytical model, as shown in **Figure 9**.

2.1 Dimensionless type-curves

For general applications, type-curves are used as a diagnostic tool to assess the solution by matching the trends of observed data to the type-curves. This approach is commonly used in well testing [52]. To enable scalability of the solution for a wide range of problem conditions, type-curves are expressed in terms of dimensionless groups. In this problem, the following dimensionless variables are considered,

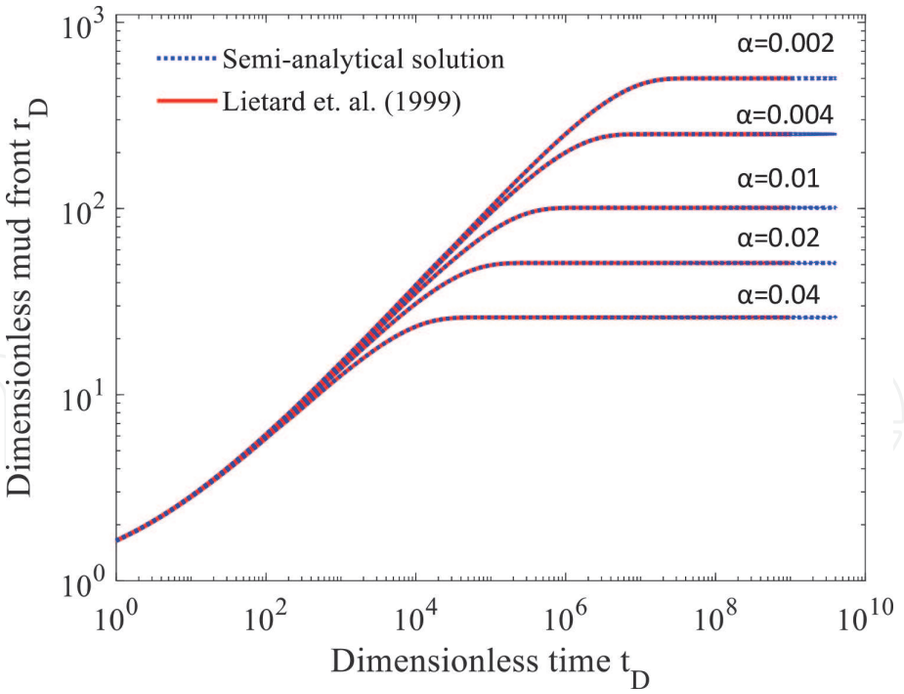

Figure 8.
Proposed semi-analytical solution compared with Liétard et al. (1999) for a Bingham plastic fluid [42].

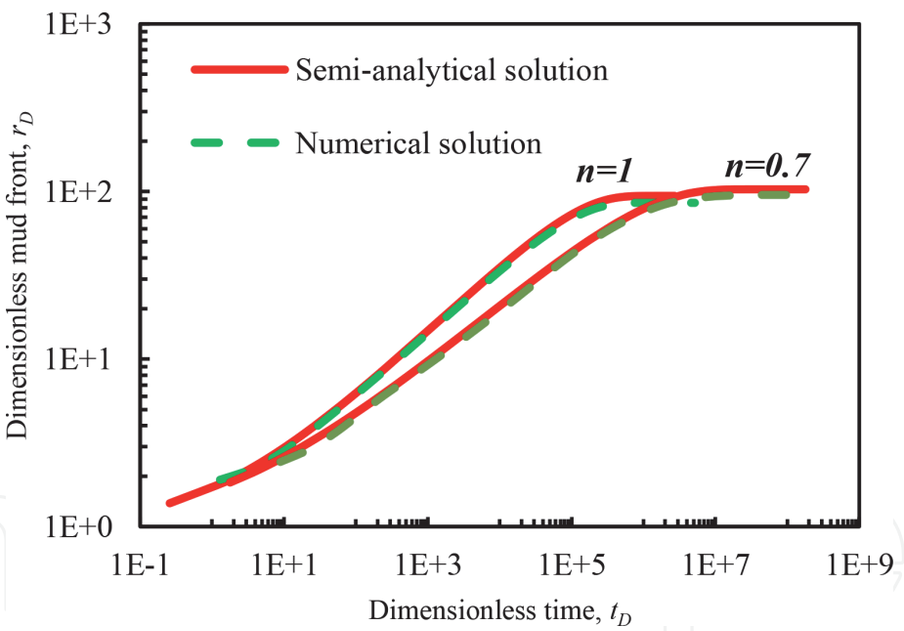

Figure 9.
Proposed semi-analytical solution compared with a finite-element model showing a good agreement [42].

$$
\begin{aligned}
r_D &= \frac{r_f}{r_w} \\
V_D &= \frac{V_m}{V_w} = \frac{\pi w\left(r_f{}^2 - r_w{}^2\right)}{\pi w r_w{}^2} = \left(\frac{r_f}{r_w}\right)^2 - 1 = r_D{}^2 - 1 \\
\alpha &= \left(\frac{2n+1}{n+1}\right)\left(\frac{2r_w}{w}\right)\left(\frac{\tau_0}{\Delta p}\right) \\
\beta &= \left(\frac{n}{2n+1}\right)\left(\frac{w}{r_w}\right)^{1+\frac{1}{n}}\left(\frac{\Delta p}{m}\right)^{\frac{1}{n}} \\
t_D &= t\beta
\end{aligned}
\tag{13}
$$

Where, r_D denotes the dimensionless radial mud-front, V_D is the dimensionless mud-loss volume, and t_D is the dimensionless time. The generated type-curves from Eq. (13) can represent a range of fluid properties, captured by two parameters. The first parameter, α, represents the mud rheological properties and flow behavior, while the second parameter, β, reflects the criteria for mud loss stoppage. The final forms of the type-curves are illustrated in **Figure 10**. These type-curves for mud-loss are more accurate than the ones proposed by Majidi et al. [37], which showed lower accuracy for small α. Comparisons of the proposed solution with Majidi et al. is plotted in **Figure 11**, which show that the simplified model by Majidi et al. could overestimate the radial distance of mud invasion.

2.2 Demonstration for real field cases

The applicability of the discussed modeling approach is demonstrated for field cases that encountered lost circulation. The field data for four wells include the leakage rates and the fluid types corresponding to Bingham plastic and Herschel-Bulkley fluids. Two modeling approaches are discussed, where the first is a deterministic approach that is matched with the proposed analytical solution, and the second is a probabilistic approach based on Monte Carlo simulations. The utilization of the probabilistic approach is motivated by the subsurface uncertainty of the downhole parameters.

2.2.1 Field case 1

The lost circulation data correspond to two wells, Machar 18 and Machar 20 in Machar field in North Sea [33]. The fluid loss occurred due to the presence of natural fractures. Using the proposed type-curves, the fracture apertures were

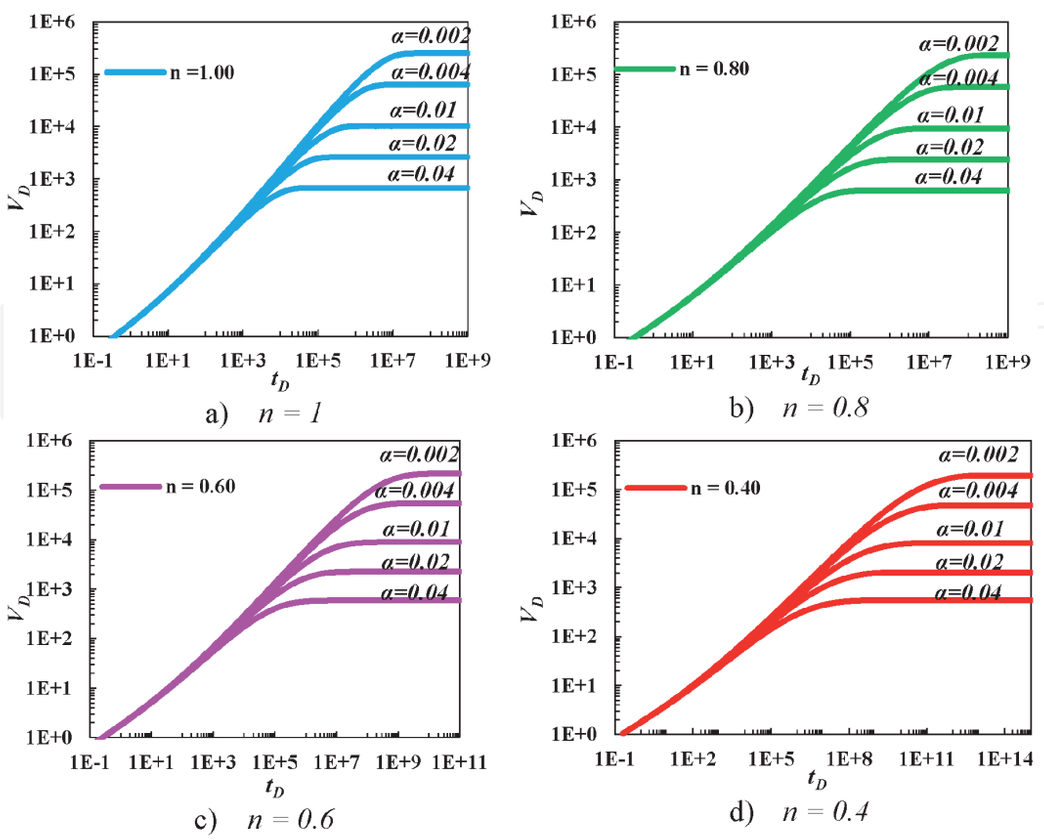

Figure 10.
Dimensionless type-curves showing dimensionless mud loss volume versus dimensionless elapsed time for a set of nand α [42].

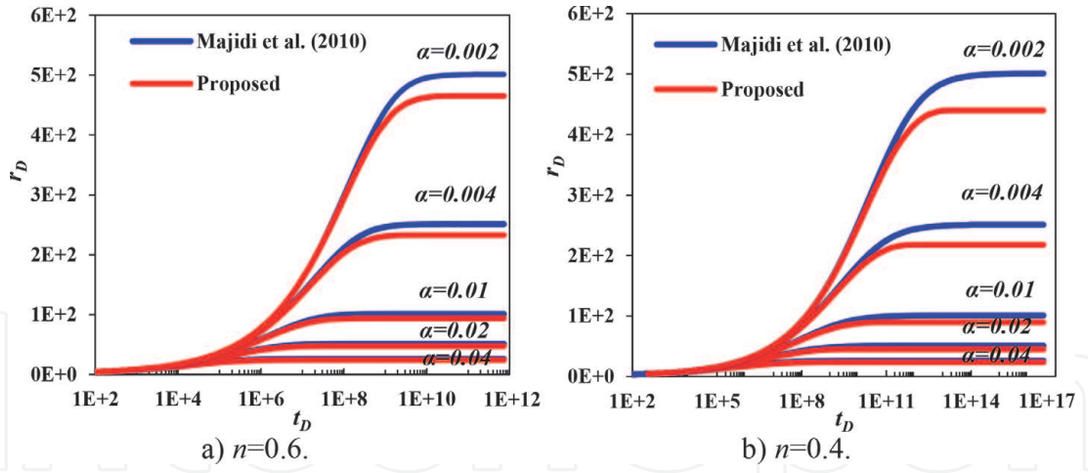

Figure 11.
Comparison between the proposed solution and the one by Majidi et al., which tends to overestimate the invasion distance for low values of α [42].

determined to be 0.42 and 0.61 mm, respectively. Both wells are plotted with the semi-analytical trends **Figure 12**. The relevant fluid and formation properties are given in **Table 2**.

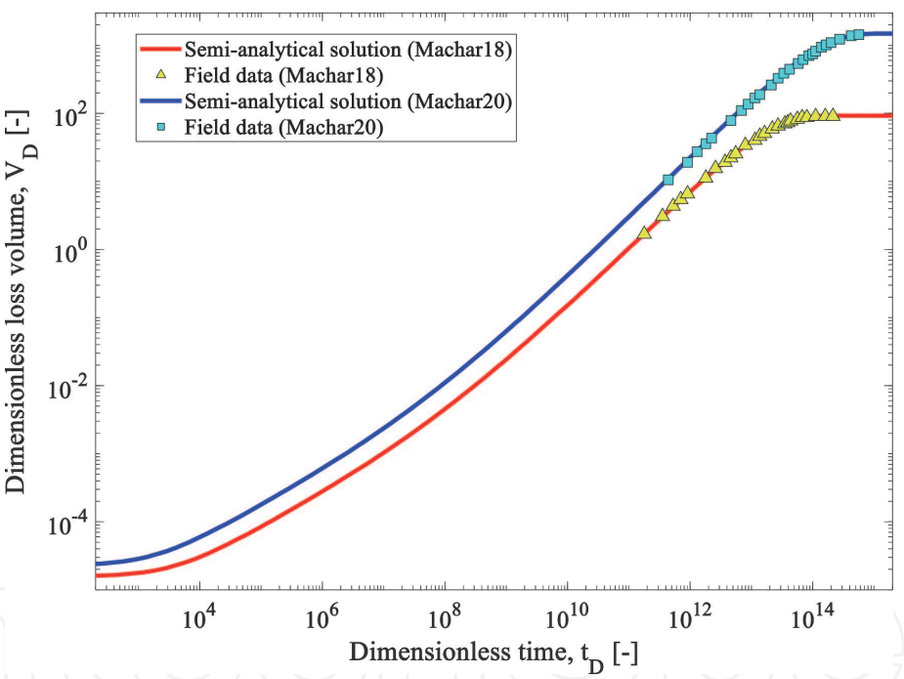

Figure 12.
Real field data matched with the semi-analytical solutions for two wells; well data are from Lietard et al. [33].

Property	Machar 18	Machar 20
Dimensionless parameter α	0.00215	0.0006436
Fracture aperture *w* [mm]	0.425	0.616
Fracture aperture *w* [mm]	0.42	0.64
Flow behavioral index	1	
Fluid yield stress [Pa]	9.34	
Fluid plastic viscosity [Pa.s]	0.035	

Table 2.
Fluid properties and fracture aperture for the two wells.

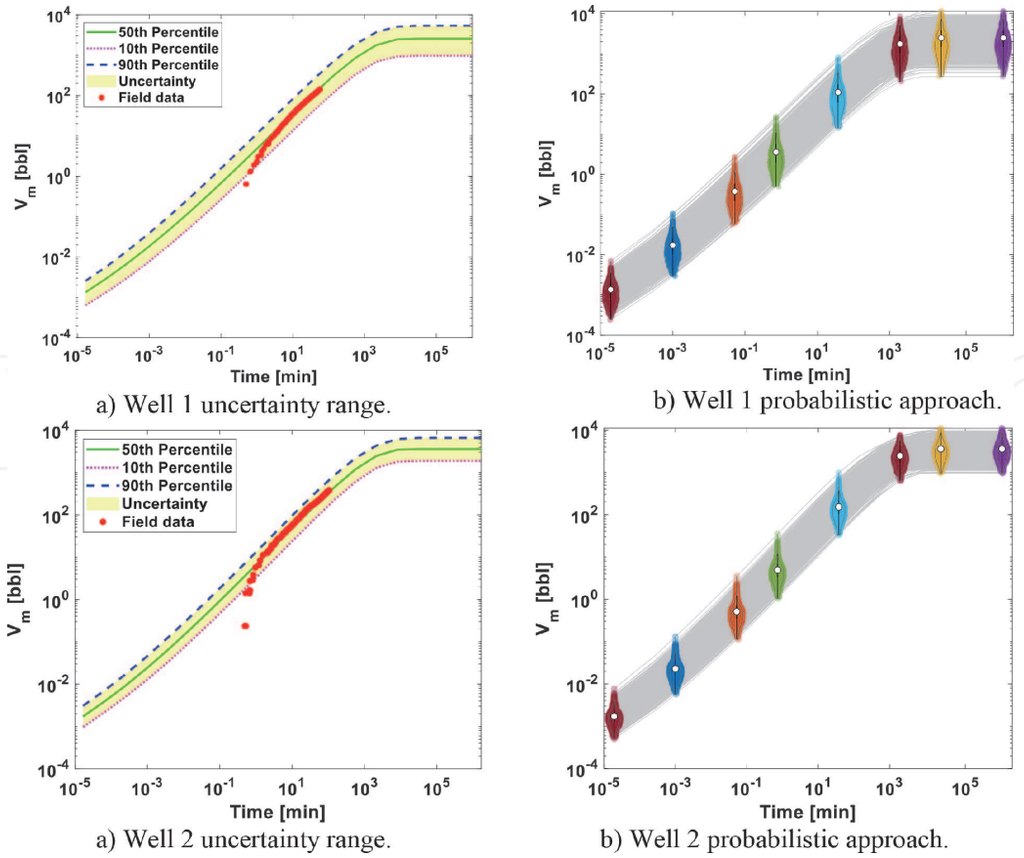

Figure 13.
Both wells are plotted cumulative mud loss volume versus time showing uncertainty plots (a) and (c), and violin distributions at selected time points (b) and (d) for well 1 and 2 respectively [42].

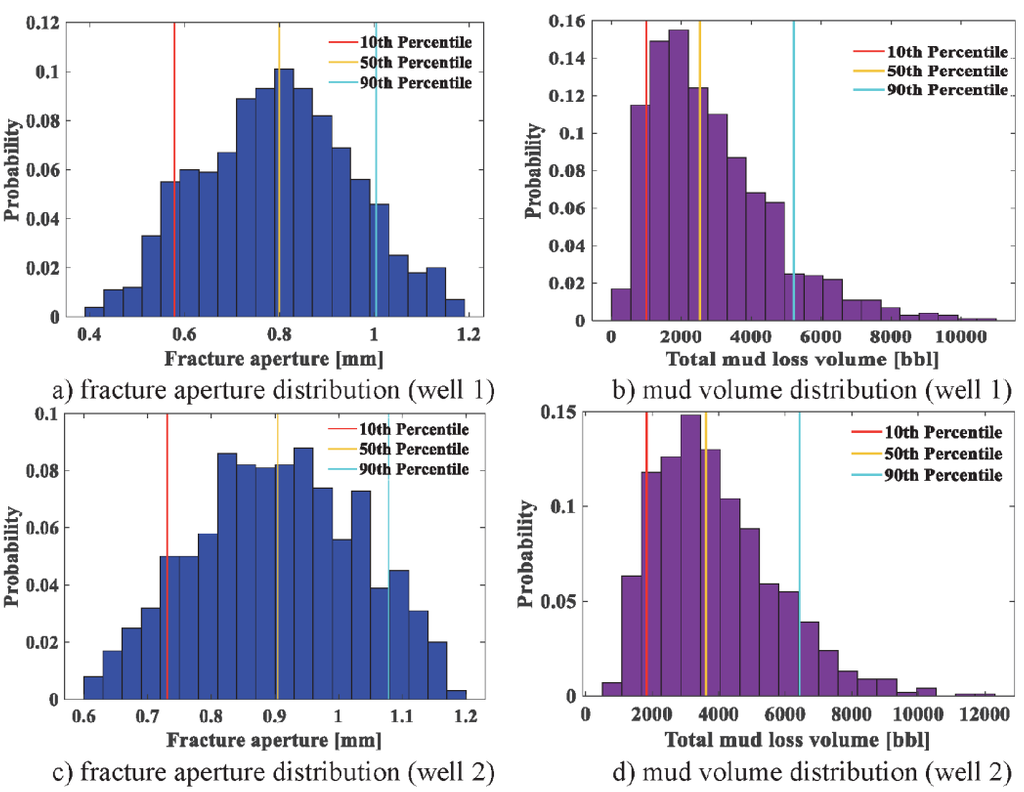

Figure 14.
Well 1 ((a) and (b)) and well 2 ((c) and (d)) output results showing average hydraulic fracture aperture in mm *can be obtained from the mud-loss analysis plus maximum cumulative mud loss volume [42].*

Property	Well 1&2
Pressure difference [MPa]	4.83–5.51
Flow behavioral index	0.94
Consistency [Pa.s^n]	3.83
Fluid yield stress [Pa]	4.02

Table 3.
Wells condition and fluid properties for field case 2 at surface conditions.

2.2.2 Field case 2

In this case, two sets of data were reported for two wells in the Gulf of Mexico [53]. The drilling fluid is Herschel-Bulkley fluid. The leakage data is provided as a volumetric flow rate in gallon per minute versus time. The provided data is converted into volumetric flow rates in m^3 per second as a function of time. Due to the uncertainty of subsurface parameters such as pressure drop, and rock properties, the semi-analytical solution is combined Monte Carlo simulations. The solutions and the data match are shown in **Figure 13**. Various useful information can be generated from these simulations. For instance, the uncertainty range of the hydraulic fracture aperture for the natural fractures can be predicted. Furthermore, the total mud-loss volumes can be estimated in the form of a histogram covering the range of uncertainty for P10, P50, and P90, percentiles, as shown in **Figure 14**. The relevant data are provided in **Table 3**.

3. Experimental study

The flow of drilling mud into an artificial fracture was studied by Majidi et al. [54]. The fracture consisted of two horizontal plates placed in parallel within a 1 mm opening, mimicking a fracture aperture. An illustration and photograph of the experimental apparatus are shown in **Figure 15**. Different fluid types and flow conditions were investigated. The inner hole, used for fluid injection, is 3 inches (in) in diameter located at the center of the upper plate. The radius of the fracture plates is 36 in. Pressure transducers were installed at different locations along the fracture radial distance. The pressure at the fracture outlet was maintained at the

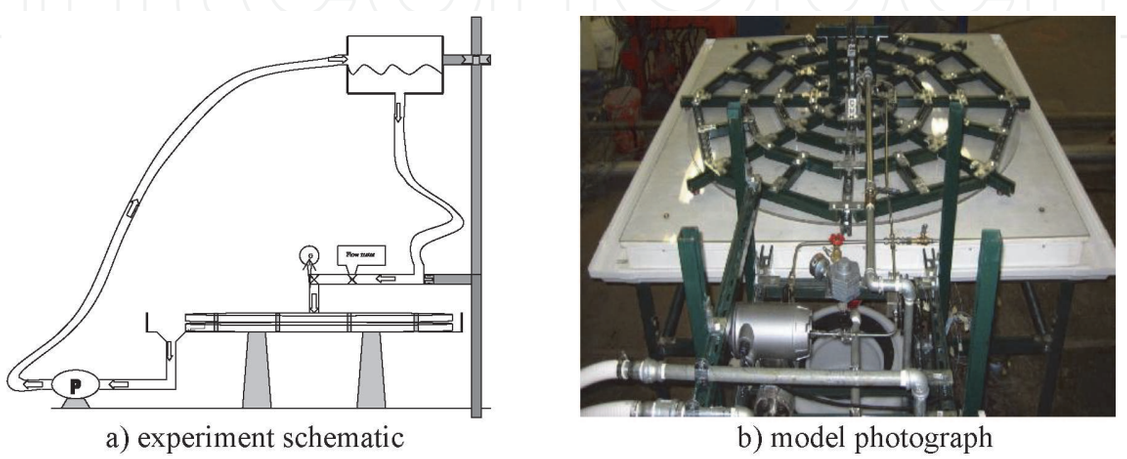

Figure 15.
Experimental setup showing a schematic view (a) and a photograph (b) of an experimental setup consisting of two parallel plates separated by a gap [54] (with permission from the author).

atmospheric conditions. The non-Newtonian fluid was injected by gravity from a supply tank placed at a certain height.

3.1 Steady-state flow test

Fluids were injected into the fracture system at a constant rate in a circulation mode until the steady-state condition was reached for the pressure within the fracture. The experiment was conducted with two different fluids, as provided in **Table 4**. A semi-analytical solution was developed to model steady-state radial flow for non-Newtonian fluids following a Yield-Power Law model described in the following,

$$-\frac{dp}{dr} = \frac{kQ_{in}^{n}}{\left[4\pi\left(\frac{n}{2n+1}\right)\left(\frac{w}{2}\right)^{2}\right]^{n}\left(\frac{w}{2}\right)} + \left(\frac{2n+1}{n+1}\right)\left(\frac{2\tau_0}{w}\right) \tag{14}$$

Where differential pressure with respect to radial distance $\frac{dp}{dr}$ equals to the operating conditions for inlet flow rate Q_{in}, fluid properties, and fracture aperture w. The fluid is characterized by fluid yield stress τ_0, consistency factor k, and flow behavioral index n. The limitation of this semi-analytical model is related to the assumption of constant fracture aperture, which is inconsistent with the varying fracture aperture caused by a slight deformation of the upper plate due to fluid pressure during injection.

A commercial simulator (COMSOL®) was used to investigate the effect of fracture wall deformation on the pressure behavior [55]. The results of viscosity and corresponding shear at three locations with respect to radial distance, reflecting shear thinning and thickening effects are shown in **Figure 16**.

3.2 Fracture ballooning effect

Fracture deformation and ballooning due to increased fluid pressure inside the fracture could occur [55]. Majidi et al. reported that there is a deformation happening somewhere between inlet and outlet caused by force distribution from fluid pressure. The physics behind fracture ballooning is related to mechanical deformation of the fracture resulting from fluid pressure and the surrounding stress field, causing the fracture to reshape its aperture by either opening or closing [56–58]. Simulations are used to investigate the fracture wall deformation and the corresponding pressure response. Simulations were conducted for deformed fracture plates, as illustrated in **Figure 17**. The results of pressure profiles for the deformed plate are in good agreement with the experimental measurements, as observed in **Figure 18**.

Fluid Name	**Polymer solution (Pack)**	**Xanthan gum**
Yield-Stress, τ_0 [Pa]	0	1.45
Consistency factor, k [Pa.s^n]	5.30	3.37
Flow Index, n [Dimensionless]	0.480	0.407
Flow Rate, Q_{in} [m^3/hr]	0.057, 0.113, 0.237	0.025, 0.057, 0.123
Flow Rate, Q_{in} [US gal/min]	0.25, 0.50, 1.00	0.11, 0.25, 0.54

Table 4.
Rheological properties for two fluids used in steady-state flow test [54].

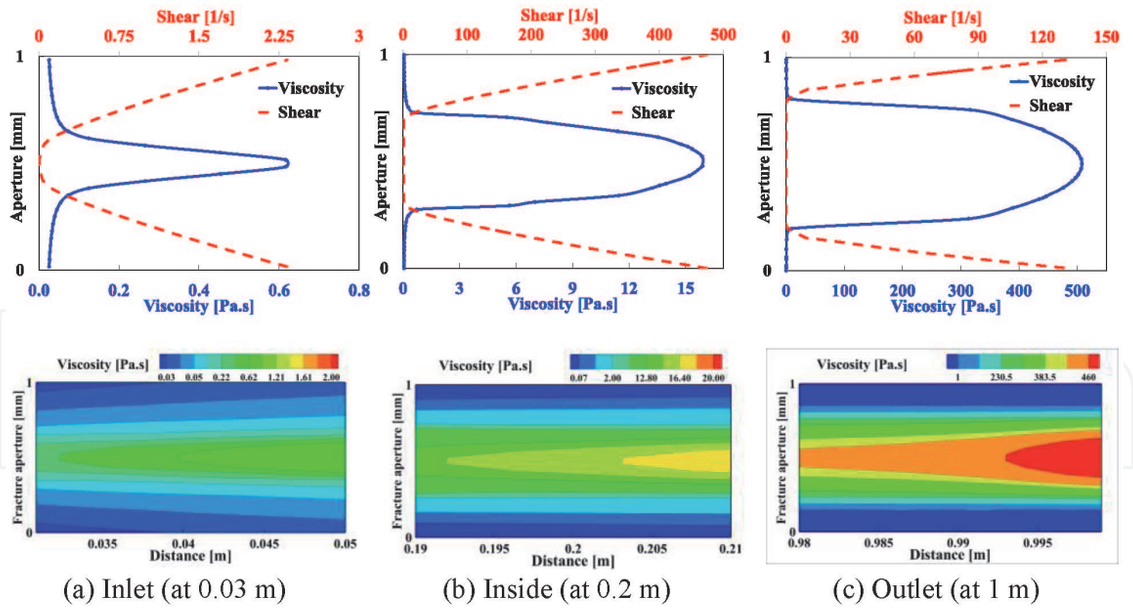

Figure 16.
Fluid viscosity and shear rate along the fracture aperture at the inlet (0.03 m), inside (0.2 m), and outlet (1 m). The bottom plots show the corresponding viscosity color maps from the numerical model.

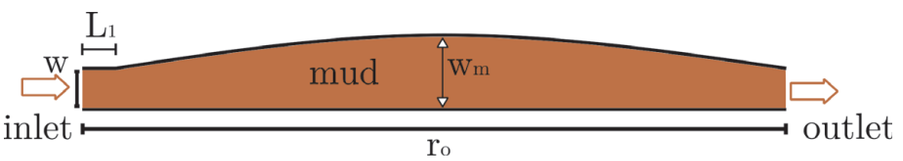

Figure 17.
Cross-section of proposed geometry showing a parabolic-shape deformation for upper plate [55].

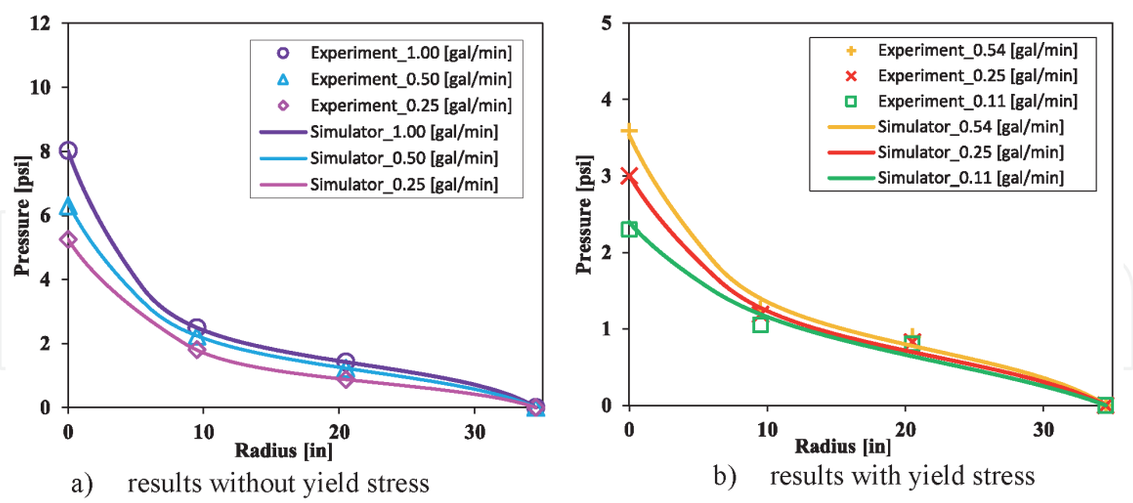

Figure 18.
Match results of experimental data and simulations for the six cases at various flow rates, without fluid yield stress (a) with yield stress (b) [55].

3.3 Plug flow test

The experiment was conducted to investigate the stoppage of flow invasion as a result of the fluid yield stress. The final invasion distances for two fluids were measured in the radial fracture system. Different injection pressures at the inlet were tested, for which the steady-state mud invasion front was measured. This

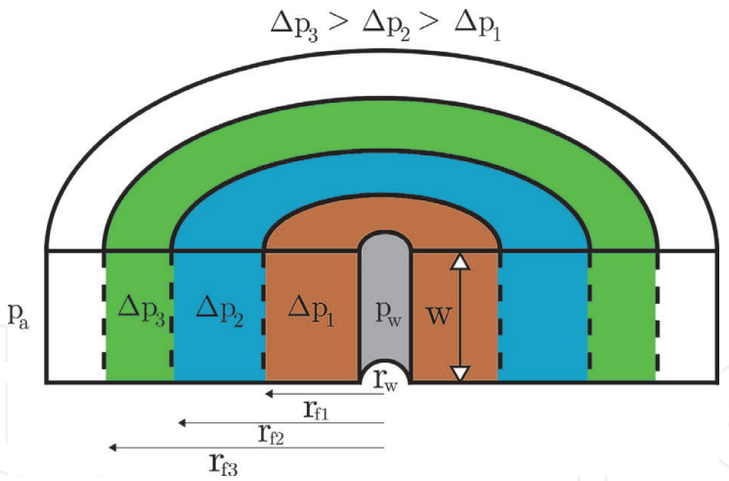

Figure 19.
Illustration of a plug-test experiment showing mud-invasion fronts r_f in different colors at different applied pressure.

Fluid Name	Xanthan gum 40 [g/L]	Xanthan gum 30 [g/L]
Yield-Stress, τ_0 [Pa]	13.9	9.6
Consistency factor, k [Pa.s^n]	4	5.5
Flow Index, n [Dimensionless]	0.34	0.315
Parabola vertex, w_m [mm]	1.5	1.25

Table 5.
Fluid properties used in plug flow experiment.

experiment is illustrated in **Figure 19**. Understanding this effect is required to predict the maximum mud loss volume [59]. The two fluids are described in **Table 5**.

Because of the fracture ballooning, the aperture is not constant, as shown in **Figure 18**. The equation used to describe the varying aperture $w(r)$as a function of radial distance$r$ is given in Eq. (15). The maximum opening of fracture aperture is captured by the parameter w_m, distance from inlet where no occurred deformation is defined by L_1 and initial aperture where no deformation occurred is w_i. Inlet and outlet radii are r_w and r_o.

$$w(r) = \begin{cases} w_i & \text{if} \quad r_w \le r < L_1 \\ (w_m - w_i)\left[1 - \dfrac{\left(r - r_w - L_1 - \frac{r_o - r_w - L_1}{2}\right)^2}{\left(\frac{r_o - r_w - L_1}{2}\right)^2}\right] + w_i & \text{if} \quad r \ge L_1 + r_w \end{cases} \tag{15}$$

When the mud stops, the flow rate is zero, that is,

$$\frac{dp}{dr} = \frac{2\tau_0(1+2m)}{(1+m)w} \tag{16}$$

Integrating the above equation over the fracture to get,

$$\int_{r_w}^{r_f} p(r)\mathrm{d}r = \int_{r_w}^{L_1} p(r)\mathrm{d}r + \int_{L_1}^{r_f} p(r)\mathrm{d}r \tag{17}$$

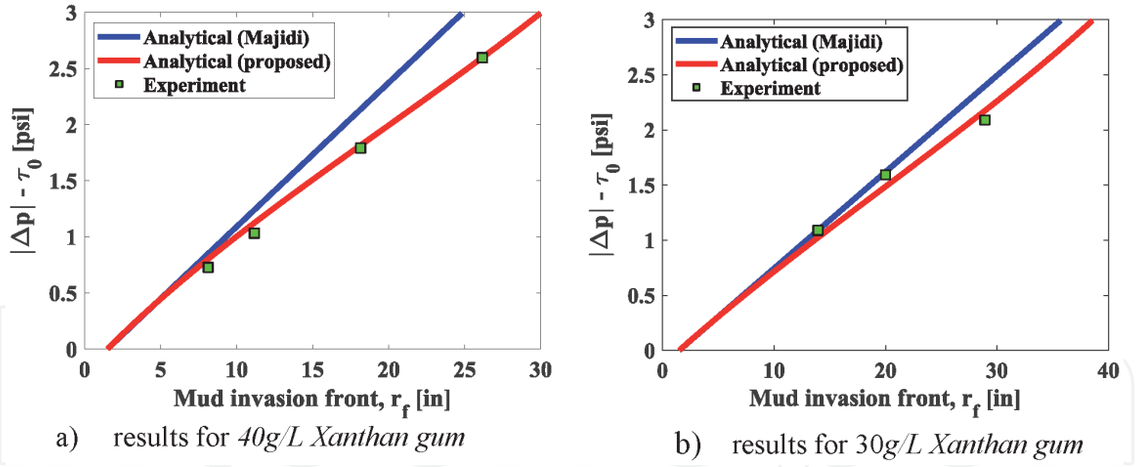

Figure 20.
Mud invasion results for two fluids with yield stress (40 g/L xanthan gum (a); 30 g/L xanthan gum (b)), and comparison with the a different model [55].

After integration of Eq. (17), the invasion radius, r_f, is expressed in terms of the fluid rheological properties and the fracture geometry, as follows,

$$r_f = \frac{1}{2}(L_1 + r_o + r_w) + \frac{\frac{1}{2}w_m}{\sqrt{\frac{(w_i - w_m)w_m}{(L_1 - r_o + r_w)^2}}} \tan\left[\frac{(-2(1+2m)(L_1 - r_w)\tau_0 + \Delta p(1+m)w_i)\sqrt{\frac{(w_i - w_m)w_m}{(L - r_o + r_w)^2}}}{(1+2m)\tau_0 w_i} + \arctan\left[\frac{(L_1 - r_o - r_w)}{w_m}\sqrt{\frac{(w_i - w_m)w_m}{(L_1 - r_o + r_w)^2}}\right]\right] \quad (18)$$

The solution of this equation is plotted along with experimental measurements in **Figure 20**. The results are in excellent agreement with the experimental data and show significant improvement to the model by Majidi et al. [37], which assumes uniform fracture and, therefore, ignores fracture deformation.

4. Conclusions

Lost circulation during drilling operations is a common problem that requires immediate intervention to circumvent fluid loss. Diagnostic tools, based on simplified input data such as fluid properties, pressure, and rate trends, can be quickly deployed to quantify uncertainties related to the fluid leakage into the subsurface formation and to perform predictions. Semi-analytical solutions are used to model the leakage behavior of general Herschel-Bulkley fluids into a horizontal infinite-acting fracture, mimicking the effect of a fractured formation. The approach is applicable to different types of non-Newtonian fluids, including yield stress shear-thinning and shear-thickening fluids. The model could predict the trend of mud leakage in a system with horizontal fractures as a function of time. It can estimate the effective hydraulic aperture of the fracture, the ultimate total mud-loss volume, and the expected duration before the leakage stalls, if conditions allow.

Dimensionless groups are used to generate type-curves, which can provide quick diagnostics about the leakage behavior from matching the type-curve trends without a need for simulations. The applicability of the model was demonstrated for four wells from two different fields. A numerical procedure was described to couple the model with Monte-Carlo simulations to perform predictions under uncertainties. This approach is a practical diagnostic tool to perform quick predictions and to optimize LCM selection.

Acknowledgements

The authors thank King Abdullah University of Science and Technology (KAUST), and Ali I. Al-Naimi Petroleum Engineering Research Center (ANPERC) for supporting this work.

Conflict of interest

The authors declare no conflict of interest.

Nomenclature

$\mathbf{v}$	velocity vector, m/s
A	defined constant
B	defined constant
D	defined constant
d	normal derivative
$\mathbf{g}$	gravitational acceleration, m/s^2
$\mathbf{I}$	identity matrix
L_1	distance from inlet where no occurred deformation along the plate, m
m	consistency multiplier, kg/(Pa.s^n)
n	flow behavioral index
p	pressure, psi
p_f	formation pressure, psi
p_w	wellbore pressure, psi
Q_{free}	volumetric flow rate in free region, m^3/s
Q_{plug}	volumetric flow rate in plug region, m^3/s
Q_{total}	total volumetric flow rate, m^3/s
r	radial distance (variable argument), m
r_D	dimensionless mud front radius, m
r_f	mud front radius, m
r_w	wellbore radius, m
t	time, min
t_D	dimensionless time
V_D	dimensionless mud loss volume
V_m	cumulative mud loss volume, bbl
V_w	wellbore volume due to fracture aperture, bbl
v_r	radial velocity, m/s
$v_{r,plug}$	radial velocity in plug region (non-deformed region), m/s
$v_{r,free}$	radial velocity profile in the free deformed region, m/s
w	fracture aperture, mm

$w(r)$	varying aperture as a function of radial distance, mm
w_i	initial fracture aperture, mm
w_m	maximum opening of fracture aperture, mm
z	z-direction in radial coordinate, m
z_{plug}	height of plug region profile, m
α	dimensionless parameter
β	dimensionless parameter
∂	partial derivative
$\boldsymbol{\gamma}$	shear rate, 1/s
Δp	pressure drop, psi
$\boldsymbol{\mu}_0$	viscosity due to fluid yield stress, Pa.s
$\boldsymbol{\mu}_{eff}$	effective viscosity, Pa.s
ρ	density
$\boldsymbol{\tau}$	shear stress tensor, Pa
$\tau(z,r)$	shear stress component as a function of z and r, Pa
τ	shear stress, Pa
τ_0	fluid yield stress, Pa

Author details

Rami Albattat and Hussein Hoteit*
Physical Science and Engineering Division, King Abdullah University of Science and Technology, Thuwal, Saudi Arabia

*Address all correspondence to: hussein.hoteit@kaust.edu.sa

References

[1] N.R. Council. Drilling and excavation technologies for the future. In: Chapter 3. National Academies Press; 1994. pp. 12-29 https://doi.org/https://doi.org/10.17226/2349

[2] J. Amadi-echendu, A.E. Yakubu, Asset Operations: Non-productive Times During Oil Well Drilling, (2016) 43–48. https://doi.org/10.1007/978-3-319-27064-7.

[3] B. Rehm, J. Schubert, A. Haghshenas, A. Paknejad, J. Hughes, Managed Pressure Drilling, Gulf Publ. Co. (2008).

[4] Bolton et al., Dramatic incidents during drilling at Wairakei Geothermal Field, New Zealand, Geothermics. 38 (2009) 40–47.

[5] D. Reid, S. Rosenberg, M. Montgomery, M. Sutherland, P. York, W. Intl, Drilling-Hazard Mitigation—Reducing Nonproductive Time by Application of Common Sense and High-Value-Well Construction Techniques, Offshore Technol. Conf. (2006).

[6] J. Willis, Wynne, Combating Lost Circulation While Cementing in the Mid-Continentt, Am. Pet. Inst. (1959).

[7] R.A. Silent, Circulation Losses, Drill. Prod. Pract. (1936).

[8] E. Lécolier, B. Herzhaft, L. Rousseau, L. Néau, B. Quillien, J. Kieffer, Development of a nanocomposite gel for lost circulation treatment, SPE - Eur. Form. Damage Conf. Proceedings, EFDC. (2005) 327–335. https://doi.org/10.2523/94686-ms.

[9] J. Seyedmohammadi, The effects of drilling fluids and environment protection from pollutants using some models, Model. Earth Syst. Environ. 3 (2017) 23. https://doi.org/10.1007/s40808-017-0299-7.

[10] F.K. Saleh, C. Teodoriu, C.P. Ezeakacha, S. Salehi, Geothermal Drilling : A Review of Drilling Challenges with Mud Design and Lost Circulation Problem, (2020) 1–8.

[11] S. Al Maskary, A. Abdul Halim, S. Al Menhali, Curing losses while drilling & cementing, in: Abu Dhabi Int. Pet. Exhib. Conf., 2014.

[12] N. Droger, K. Eliseeva, L. Todd, C. Ellis, O. Salih, N. Silko, E. Al, Degradable fiber pill for lost circulation in fractured reservoir sections, in: IADC/SPE, 2014.

[13] A. Fox, Can Geomechanics Improve Your Drilling and Completions?, 2018.

[14] U. Arshad, B. Jain, M. Ramzan, W. Alward, L. Diaz, I. Hasan, A. Aliyev, C. Riji, Engineered Solution to Reduce the Impact of Lost Circulation During Drilling and Cementing in Rumaila Field, Iraq, in: International Petroleum Technology Conference, Doha, Qatar, 2015. https://doi.org/10.2523/iptc-18245-ms.

[15] J. Abdollahi, I.M. Carlsen, S. Mjaaland, P. Skalle, A. Rafiei, S. Zarei, Underbalanced drilling as a tool for optimized drilling and completion contingency in fractured carbonate reservoirs, SPE/IADC Underbalanced Technol. Conf. Exhib. - Proc. (2004) 195–204. https://doi.org/10.2523/91579-ms.

[16] M. Ameen, Fracture and in-situ stress patterns and impact on performance in the Khuff structural prospects, eastern offshore Saudi Arabia, Mar Pet. Geol. 50 (2014).

[17] D. Denney, Controlling Lost Circulation in flowing HP/HT Wells: Case History, JPT, J. Pet. Technol. 56 (2004) 55–56. https://doi.org/10.2118/0104-0055-jpt.

[18] Schlumberger, Lost Circulation Solution Saves Time and USD 3.3 Million for Chevron, Schlumberger. (2011).

[19] E.B. Nelson, D. Guillot, Well Cementing: Second Edition, Schlumberger, Texas, 2006.

[20] A. Lavrov, Lost circulation: Mechanisms and solutions, 2016. h ttps://doi.org/10.1016/C2015-0-00926-1.

[21] V. Dokhani, Y. Ma, Z. Li, T. Geng, M. Yu, Transient effects of leak-off and fracture ballooning on mud loss in naturally fractured formations, 53rd U. S. Rock Mech. Symp. (2019).

[22] A. Ali, C.L. Kalloo, U.B. Singh, Preventing lost circulation in severely depleted unoonsolidated sandstone reservoirs, SPE Repr. Ser. (1997) 103–109. doi:10.1016/0148-9062(94)91150-9.

[23] D.J. Attong, U.B. Singh, G. Teixeira, Successful use of a modified MWD tool in a high-concentration LCM mud system, SPE Drill. Complet. 10 (1995) 22–26. doi:10.2118/25690-PA.

[24] K. Knudsen, G.A. Leon, A.E. Sanabria, A. Ansari, R.M. Pino, First application of thermal activated resin as unconventional LCM in the Middle East, Soc. Pet. Eng. - Abu Dhabi Int. Pet. Exhib. Conf. ADIPEC 2015. (2015) 1–8. doi:10.2118/177430-ms.

[25] M. Olsen, G. Lende, K. Rehman, P. Haugum, J. Mo, G. Smaaskjar, R. Næss, Innovative and established LCM cementing solutions combined to create novel LCM cementing fluid train, Soc. Pet. Eng. - SPE Norw. One Day Semin. 2019. (2019). doi:10.2118/195622-ms.

[26] J. Luzardo, E.P. Oliveira, P.W.J. Derks, R.V. Nascimento, A.P. Gramatges, R. Valle, I.G. Pantano, F. Sbaglia, K. Inderberg, Alternative lost circulation material for depleted reservoirs, in: OTC Bras., Offshore Technology Conference, 2015. doi: 10.4043/26188-MS.

[27] C.G. Dyke, Bailin Wu, D. Milton-Taylor, Advances in characterizing natural-fracture permeability from mud- log data, SPE Form. Eval. 10 (1995) 160–166. doi:10.2118/25022-pa.

[28] J. NORMAN, Coriolis sensors open lines to real-time data, Drill. Contract. 67 (2011) 0–3.

[29] C.E. Bannister, V.M. Lawson, Role of cement fluid loss in wellbore completion, Proc. - SPE Annu. Tech. Conf. Exhib. 1985-Septe (1985). doi: 10.2523/14433-ms.

[30] R. Bruckdorfer, A. Gleit, Static Fluid Loss Model, SPE Gen. (1988) 20. https:// doi.org/.

[31] F. Sanfillippo, M. Brignoli, F.J. Santarelli, C. Bezzola, Characterization of Conductive Fractures While Drilling, SPE Eur. Form. Damage Conf. (1997) 319–328. doi:10.2118/38177-ms.

[32] R. Maglione, A. Marsala, Drilling mud losses: problem analysis, AGIP Internal Report, 1997.

[33] O. Liétard, T. Unwin, D.J. Guillot, M.H. Hodder, Fracture width logging while drilling and drilling mud/loss-circulation-material selection guidelines in naturally fractured reservoirs, SPE Drill. Complet. 17 (1999) 237–246.

[34] F. Civan, M. Rasmussen, Further discussion of fracture width logging while drilling and drilling mud/loss-circulation-material selection guidelines in naturally fractured reservoirs, SPE Drill. Complet. 17 (2002) 249–250.

[35] S. Sawaryn, Discussion of fracture width logging while drilling and drilling mud/loss-circulation-material selection guidelines in naturally fractured

reservoirs, SPE Drill. Complet. 4 (2002) 247–248.

[36] J. Huang, D.V. Griffiths, S.-W. Wong, Characterizing Natural-Fracture Permeability From Mud-Loss Data, SPE J. 16 (2011) 111–114. doi:10.2118/139592-PA.

[37] Majidi, S.Z. Miska, M. Yu, L.G. Thompson, J. Zhang, Quantitative Analysis of Mud Losses in Naturally Fractured Reservoirs: The Effect of Rheology, SPE Drill. Complet. December 2 (2010) 509–517. doi: 10.2118/114130-PA.

[38] A.C. Hindmarsh, P.N. Brown, K.E. Grant, S.L. Lee, R. Serban, D.E. Shumaker, C.S. Woodward, SUNDIALS: Suite of nonlinear and differential/algebraic equation solvers, ACM Trans. Math. Softw. 31 (2005) 363–396. doi: 10.1145/1089014.1089020.

[39] A. Nasiri, A. Ghaffarkhah, M. Keshavarz Moraveji, A. Gharbanian, M. Valizadeh, Experimental and field test analysis of different loss control materials for combating lost circulation in bentonite mud, J. Nat. Gas Sci. Eng. 44 (2017) 1–8. doi:10.1016/j.jngse.2017.04.004.

[40] S. Yousefirad, E. Azad, M. Dehvedar, P. Moarefvand, The effect of lost circulation materials on differential sticking probability: Experimental study of prehydrated bentonite muds and Lignosulfonate muds, J. Pet. Sci. Eng. 178 (2019) 736–750.

[41] M. Khafaqa, Experimental Study on Effectiveness of Lost Circulation Materials to Mitigate Fluid Losses, MONTANUNIVERSITÄT LEOBEN, 2016.

[42] R. Albattat, H. Hoteit, A Semi-Analytical Approach to Model Drilling Fluid Leakage Into Fractured Formation, 2020. https: //doi.org/https://arxiv.org/abs/2011.04746.

[43] H. Hoteit, A. Firoozabadi, An efficient numerical model for incompressible two-phase flow in fractured media, Adv. Water Resour. 31 (2008) 891–905. doi:10.1016/j.advwatres.2008.02.004.

[44] B. Koohbor, M. Fahs, H. Hoteit, J. Doummar, A. Younes, B. Belfort, An advanced discrete fracture model for variably saturated flow in fractured porous media, Adv. Water Resour. 140 (2020) 103602. doi:10.1016/j.advwatres.2020.103602.

[45] M.B. Smith, C.T. Montgomery, Hydraulic fracturing, Crc Press, 2015. doi:10.1201/b16287.

[46] Z. Ben-Avraham, M. Lazar, Z. Garfunkel, M. Reshef, A. Ginzburg, Y. Rotstein, U. Frieslander, Y. Bartov, H. Shulman, Structural styles along the Dead Sea Fault, in: D.G. Roberts, A.W.B. T.-R.G. and T.P.P.M. Bally Cratonic Basins and Global Tectonic Maps (Eds.), Reg. Geol. Tectonics, Elsevier, Boston, 2012: pp. 616–633. doi:10.1016/B978-0-444-56357-6.00016-0.

[47] F. Irgens, Rheology and non-newtonian fluids, Springer International Publishing, 2014.

[48] D. Cioranescu, V. Girault, K.R. Rajagopal, Mechanics and Mathematics of Fluids of the Differential Type, Springer, 2016. doi:10.1007/978-3-319-39330-8.

[49] R.L. Panton, Incompressible flow, John Wiley & Sons, 2013. https://doi.org/https://doi.org/10.1002/9781118713075.ch10.

[50] T. Hemphil, A. Pilehvari, W. Campos, Yield-power law model more accurately predicts mud rheology, Oil Gas J. 91 (1993) 45–50.

[51] V.C. Kelessidis, R. Maglione, C. Tsamantaki, Y. Aspirtakis, Optimal determination of rheological parameters

for Herschel-Bulkley drilling fluids and impact on pressure drop, velocity profiles and penetration rates during drilling, J. Pet. Sci. Eng. 53 (2006) 203–224. https://doi.org/10.1016/j.petrol.2006.06.004.

[52] J. Lee, Well Testing, Society of Petroleum Engineers, 1982. https://store. spe.org/Well-Testing–P179.aspx (accessed June 29, 2020).

[53] R. Majidi, Modeling of Yield-power law drilling fluid losses in naturally fractured formations, The university of Tulsa, 2008.

[54] R. Majidi, S.Z. Miska, R. Ahmed, M. Yu, L.G. Thompson, Radial flow of yield-power-law fluids: Numerical analysis, experimental study and the application for drilling fluid losses in fractured formations, J. Pet. Sci. Eng. 70 (2010) 334–343. https://doi.org/10.1016/j.petrol.2009.12.005.

[55] R. Albattat, H. Hoteit, Modeling yield-power-law drilling fluid loss in fractured formation, J. Pet. Sci. Eng. 182 (2019) 106273. doi:10.1016/j.petrol.2019.106273.

[56] S. Baldino, S.Z. Miska, E.M. Ozbayoglu, A novel approach to borehole-breathing investigation in naturally fractured formations, SPE Drill. Complet. 34 (2019) 27–45.

[57] M.A. Ojinnaka, J.J. Beaman, Full-course drilling model for well monitoring and stochastic estimation of kick, J. Pet. Sci. Eng. 166 (2018) 33–43. https://doi.org/doi:10.1016/j.petrol.2018.03.012.

[58] Z. Yuan, D. Morrell, A.G. Mayans, Y.H. Adariani, M. Bogan, Differentiate Drilling Fluid Thermal Expansion, Wellbore Ballooning and Real Kick during Flow Check with an Innovative Combination of Transient Simulation and Pumps off Annular Pressure While Drilling, in: IADC/SPE Drill. Conf. Exhib., Society of Petroleum Engineers, 2016.

[59] Y. Sun, Near-Wellbore Processes in Naturally Fractured or Weakly Consolidated Formations Near-Wellbore Processes in Naturally Fractured or, (2017).